4-28-2023

Constraining H0 Via Extragalactic Parallax

Nicholas Ferree
University of Richmond, nicholas.ferree@richmond.edu

Constraining H_0 Via Extragalactic Parallax

Nicolas Ferree

Honors Thesis

Submitted to:

Department of Physics
University of Richmond
Richmond, VA

April 28, 2023

Advisor: Dr. Ted Bunn

ABSTRACT

We examine the prospects for measurement of the Hubble parameter H_0 via observation of the secular parallax of other galaxies due to our own motion relative to the cosmic microwave background rest frame. Peculiar velocities make distance measurements to individual galaxies highly uncertain, but a survey sampling many galaxies can still yield a precise H_0 measurement. We use both a Fisher information formalism and simulations to forecast errors in H_0 from such surveys, marginalizing over the unknown peculiar velocities. The optimum survey observes $\sim 10^2$ galaxies within a redshift $z_{\max} = 0.06$. The required errors on proper motion are comparable to those that can be achieved by Gaia and future astrometric instruments. A measurement of H_0 via parallax has the potential to shed light on the tension between different measurements of H_0.

Key words: Astrometry and Celestial Mechanics – Proper motions – Methods: Statistical – Parallaxes – Cosmology: Distance Scale – Cosmology: Observations

1 BACKGROUND

The current benchmark model of cosmology is the ΛCDM concordance model. This model describes an expanding, spatially flat universe governed by the field equations of General Relativity (GR) that begins in a hot big bang and undergoes an inflationary period early in its existence. In this model, the mass-energy of the Universe is composed of matter, radiation, and dark energy. Early in its existence, the Universe was dominated by electromagnetic radiation; soon thereafter it was dominated by matter, and it is now dominated by dark energy in the current epoch (Ryden 2016). The dark energy component of this universe is consistent with a vacuum energy, incorporated into the model by adding a cosmological constant Λ to the GR field equations. A small percentage (roughly 17%) of the matter is the baryonic matter described by the Standard Model of particle physics; however, most of the matter is cold dark matter (Planck Collaboration et al. 2020). While the exact nature of this matter is unknown, it appears to have very weak electromagnetic interactions (hence the matter being "dark") and non-relativistic speeds (hence the matter being "cold") (Ryden 2016; Planck Collaboration et al. 2020). The physics of such a universe is captured by six cosmological parameters and the field equations of GR. While there is a choice of parameterization, a commonly used parameter set is $\omega_b = \Omega_b h^2, \omega_c = \Omega_c h^2, H_0, \tau, n_s, ln(10^{10} A_s)$ (these are the baryon density today, the cold dark matter density today, the expansion rate of the Universe at the current point in spacetime [1], the Thomson scattering optical depth due to reionization, scalar index for the CMB power spectrum, and the logarithmic power of the primordial curvature perturbations) (Planck Collaboration et al. 2020).

The ΛCDM model has been remarkably successful at explaining a wide range of cosmological observations. For example, an inflationary period following a hot big bang predicts the existence and statistical properties of a radiation background due to the emission of photons immediately after the universe expanded and cooled sufficiently to become transparent. This background has been redshifted to the microwave and is therefore called the cosmic microwave background (CMB). A variety of experiments have measured the power spectrum of the CMB and found it to be consistent with the theoretical predictions of ΛCDM to a very high degree of precision. Other observations supporting the ΛCDM model include the large-scale structure of the universe (i.e., the distribution of galaxies and galaxy clusters), the rotation curves of galaxies (consistent with the presence of massive dark matter haloes), and the relative abundance of baryonic elements in the observable universe (Ryden 2016; Planck Collaboration et al. 2020).

However, despite its many successes, the ΛCDM model has several theoretical and observational shortcomings. Only 4% of the universe is composed of baryonic matter; the rest of the mass-energy content is contributed by dark matter and dark energy (Planck Collaboration et al. 2020). Dark matter is not predicted by the Standard Model, and the nature of such matter is almost entirely unknown. Furthermore, despite decades of intense effort, no direct detections of dark matter have been made. Similarly, the nature of dark energy is poorly understood. While it is consistent with energy contributed by the vacuum, the cosmologically inferred value for the vacuum energy density differs from the theoretical predictions of quantum field theory by over 100 orders of magnitude (Adler et al. 1995). This shocking discrepancy has been dubbed the "vacuum catastrophe". Finally, the past few decades have seen greatly increased precision in several independent methods of measuring the Hubble constant H_0. Unfortunately, the leading two measurements (local measurements of Type Ia supernovae and analysis of the CMB) differ from each other by substantially more than their error bars, leading to a $> 5\sigma$ discrepancy known as the "Hubble tension" (Kamionkowski & Riess 2022).

Observations of Type IA supernovae allow for inference of the Hubble constant via a calibration technique known as the "distance ladder". The distance ladder uses known distances of nearby Cepheid variable stars to calibrate a period-luminosity relation for Cepheid type stars. (These distances are generally obtained by statistical parallax measurements, main sequence fitting of stellar clusters containing Cepheids, the Baade-Becker-Wesselink method, geometric analysis of eclipsing binary systems, or analysis of water masers in the active galactic nuclei of nearby galaxies hosting a Cepheid population)[2] (Yuan et al. 2022). This period-luminosity relation is then used in conjunction with measurements of higher redshift Cepheids to calibrate the intrinsic luminosity of type Ia supernovae, which are known as "standard candles". Theoretical studies of this class of supernovae

[1] We note that this parameter is often replaced with $100\theta_{MC}$, the angular scale of the sound horizon (i.e., the distance sound could travel between the big bang and recombination). In such a parameterization, H_0 is treated as a derived parameter. It is equally valid to treat H_0 as fundamental and $100\theta_{MC}$ as derived; since the parameter we are most interested in is H_0, we will follow this convention.

[2] Statistical parallax involves taking an average parallax measurement of a stellar cluster, while main sequence fitting involves fitting color vs. observed luminosity of a stellar cluster to the known color vs. intrinsic luminosity of the main stellar sequence. The Baade-Becker-Wesselink method uses the color to infer the temperature of the star and measures the radial velocity via doppler shift. Using these and the Stefan-Boltzmann law, the distance to the star may be inferred (Lazovik et al. 2019).

conclude that the physical conditions causing this type of supernova result in highly predictable intrinsic luminosities; since the luminosity of these "standard candles" can be inferred physically, comparing the observed luminosity to the intrinsic luminosity yields a distance measurement to a supernova (Wright & Li 2018). This method allows for distance measurements to a large sample of type Ia supernovae independent of redshift measurements for these objects. Combining these distance and redshift measurements therefore allows for estimation of the Hubble constant from observations of the local universe. The leading estimate of H_0 using this method is 73.04 ± 1.04 km s^{-1} Mpc^{-1}, as determined by the SH0ES and Pantheon+ collaboration (Riess et al. 2022).

The power spectrum of the CMB is very sensitive to a range of cosmological parameters. The random fluctuations in the CMB are acoustic in nature; detailed modeling of the conditions at the time of last scattering (i.e., the time when the Universe became transparent) therefore allows for a theoretical prediction of the physical size of these fluctuations. The observed angular size of these fluctuations depends on the physical size of the fluctuations and the distance between the CMB and the observer. Since the physical distance depends on the redshift and the Hubble constant, measuring the redshift of the CMB in combination with a knowledge of the physical size of the fluctuations therefore allows for estimation of the Hubble constant. The leading estimate of H_0 using this method is 67.4 ± 0.5 km s^{-1} Mpc^{-1}, as determined by the Planck collaboration (Planck Collaboration et al. 2020).

A third, newer method to estimate H_0 has been developed in recent years. This technique uses stars on the tip of the red giant branch (TTRGB) instead of supernovae as standard candles. A star at the tip of the red giant branch has achieved sufficient core temperature to cause the fusion of helium in an event known as a "helium flash". The luminosity of such a star is specified by the stellar physics of a helium flash, so all stars on the TTRGB should have very similar intrinsic luminosities (McQuinn et al. 2019). These stars may therefore be used as standard candles in a manner similar to type IA supernovae, first calibrating the intrinsic luminosity via observations of red giants whose distance is known from neighboring Cepheids and then using the derived intrinsic luminosity to infer distances to a larger catalogue of red giants. The leading estimate of H_0 using this method is $69.8 \pm 0.8 \pm 1.7$ km s^{-1} Mpc^{-1}, as determined by the Carnegie-Chicago program (Freedman et al. 2019). (The 0.8 km s^{-1} Mpc^{-1} error is statistical and the 1.7 km s^{-1} Mpc^{-1} error is systematic).

It is possible that these different measurements are simply a result of systematic errors that have not yet been discovered. However, if this tension is not due to systematics, it indicates a theoretical failure of ΛCDM and demands novel physics to explain the difference between early and late Universe measurements. Some suggestions for theoretical modifications include making the dark energy equation of state a function of cosmic time, introducing curvature to the model of the Universe, introducing more relativistic degrees of freedom (i.e., allowing more species of particles to be relativistic), adding a massive sterile neutrino component to the Universe, or adding a modification term to the Poisson and lensing equations of general relativity (often referred to as "modified gravity") (DES Collaboration et al. 2022).

It is therefore of great interest to the cosmological community to determine the source of this tension. In addition to further consideration of systematic errors of already existing methods, the community may proceed by making new, independent measurements of the Hubble constant. In this paper, we investigate the feasibility of an independent measurement of the Hubble constant via extragalactic parallax. Parallax, the apparent motion of an object due to the actual motion of the observer, is a purely geometric effect. This would allow for an estimate of H_0 from local measurements but would bypass the assumptions and calibrations required of the distance ladder, providing a robust geometric measurement of H_0 and yielding further insight into the nature of the Hubble tension.

2 OVERVIEW OF EXTRAGALACTIC PARALLAX

Parallax is a common tool to measure distances to relatively nearby astrophysical objects. Parallax distances to nearby stars form the first rung of the "distance ladder" (e.g., Luri et al. 2018, and references therein).

Because they depend only on geometry, parallax distances are particularly robust. As a result, it would be extremely desirable to use the method on cosmological scales, bypassing the other steps in the ladder. Traditional parallax, using the Earth's orbit as a baseline, results in unmeasurably small parallax angles for sources at cosmological distances. Kardashev (1986) noted that a larger signal could be obtained by using the solar system's motion relative to the cosmological rest frame to produce a longer baseline. From the cosmic microwave background dipole, we infer that our velocity relative to this frame is 78 AU yr^{-1} (Hinshaw et al. 2009), leading to a secular proper motion (i.e., change in angular position) of $(78\mu\text{as yr}^{-1})D_{\text{Mpc}}^{-1}\sin\beta$ for a source located at an angular diameter distance[3] D_{Mpc} megaparsecs in a direction making an angle β with the known CMB dipole direction.

For the near future, the uncertainty in a single parallax measurement is too high to be of use in determination of distances on a cosmological scale; however, advances in telescope technology provide the possibility of using cosmological parallax in a statistical analysis (Paine et al. 2020). Here, we analyze the usage of parallax measurements to constrain the Hubble parameter H_0. Should this method be feasible in the near future, it would provide an independent determination of H_0 that might help to resolve the current ambiguity in its value (Planck Collaboration et al. 2020; Riess et al. 2019).

In this paper, we will explore the space of design parameters for a survey of galaxy parallax measurements. We use both a Fisher formalism and simulations to determine the error in a measurement of H_0 from a given survey, taking into account both proper motion measurement errors and the peculiar velocities (i.e., velocities not due to the expansion of the universe) of the source galaxies. For redshift-limited surveys with varying numbers of galaxies and redshift limits, we determine the required precision with which proper motions need to be measured in order to yield an H_0 measurement with a given error.

Our purpose in this paper is to perform a preliminary study of the feasibility of an observation program of this sort. The calculations are based on approximations, in particular regarding the peculiar velocity field, that will have to be replaced with more sophisticated methods if and when such a survey is actually performed. We will argue below that our approach is adequate to give an initial estimate of the required errors and of the optimum survey design. The error forecasts we present are, of course, not as precise as those that would arise from a detailed simulation of a specific survey design. We regard such a detailed calculation as premature at this stage, although it will

[3] We will assume a cosmologically flat Universe throughout this paper. In a spatially curved universe, there is a distinction between the parallax distance and the angular diameter distance (Hogg 1999, and references therein). Because we focus on sources at low redshift, any corrections due to spatial curvature would be extremely small and would not affect our conclusions.

certainly be required at a later stage if attempts to measure H_0 via this method are actually made.

Some previous explorations of this possibility have focused on observations of quasars (Ding & Croft 2009; Bachchan et al. 2016). Other work, like ours, has focused on closer sources for which the predicted signal is larger (Croft 2021; Paine et al. 2020; Hall 2019). Hall (2019) develop a harmonic-space formalism for modeling the galaxy peculiar velocities, whereas we have chosen to work in real space. Croft (2021) and Paine et al. (2020) consider data sets modeled on particular present or future observing campaigns, whereas we have chosen to adopt an exploratory approach, asking what observing strategy would be optimal for this particular measurement.

We focus specifically on measuring H_0, but extragalactic proper motion surveys can be used to study a number of additional interesting questions (e.g., Darling et al. 2018, and references therein). Of particular note is the ability to measure the *acceleration* of our solar system's motion via secular aberration drift (Truebenbach & Darling 2017), which is the proper motion of sources due to the solar system's rotational motion around the galactic center. Probing the connection between the galaxy proper motion field and the matter power spectrum is also potentially of great interest (Darling & Truebenbach 2018).

The remainder of this paper is structured as follows. Section 2 contains the details of our methods, including the computation of marginalized likelihoods needed for both Fisher calculations and maximum-likelihood estimation in our simulations, along with numerous other details. Section 3 contains a summary of our results, and a discussion is found in Section 4.

3 METHODS

3.1 Assumptions

We wish to measure H_0 using parallax. Suppose that we have a sample of galaxies, each of which has a measured angular position, redshift, and proper motion.

From redshift alone, we are only able to determine a combination of H_0 and the distance to a galaxy (with some uncertainty due to the galaxy's unknown radial peculiar velocity). We then use the proper motion of the galaxy to constrain the distance alone, allowing us to separate the distance from H_0.

We begin with some simplifying assumptions. First, we assume that the error in angular position measurements is negligible compared to other errors, so we treat the angular position of each galaxy as perfectly known. Second, we assume that the velocity of the solar system with respect to the cosmic microwave background has been measured with a high degree of accuracy, so we treat it too as being perfectly known. Third, we assume that galaxies' peculiar velocities are uncorrelated and that each component of the peculiar velocity is drawn from a normal distribution with mean zero and standard deviation σ_v. While actual galaxy peculiar velocities are correlated, we will show in Section 4.5 that the error introduced by this approximation is acceptable. Fourth and finally, we assume that all noise is normally distributed with mean zero.

3.2 Likelihood Function and Priors

We place the Earth at the center of our coordinate system and suppose that our survey has N galaxies. Since the angular position of each galaxy is assumed to be known perfectly, we may associate with each galaxy j an orthonormal basis of vectors $\hat{R}_j, \hat{\theta}_j, \hat{\phi}_j$. We denote the peculiar velocity of the galaxy as $\vec{v}_j$, the peculiar velocity of the solar system as $\vec{v}_0$, and the relative peculiar velocity of the galaxy as $\vec{V}_j = \vec{v}_j - \vec{v}_0$. Therefore $V_{jr} = \vec{V}_j \cdot \hat{R}_j$, $V_{j\phi} = \vec{V}_j \cdot \hat{\phi}_j$, and $V_{j\theta} = \vec{V}_j \cdot \hat{\theta}_j$. We denote the angular diameter distance [4] to the j^{th} galaxy as R_{jA} and the comoving distance to the j^{th} galaxy as R_j . Finally, we let $Z(H_0, R_j)$ denote the cosmological redshift (i.e., the redshift in the absence of peculiar velocity) of a galaxy at distance R_j for a given value of H_0.

We may now write a function $\lambda = -2\ln(L) = -2\ln(\mathcal{L}) + \text{const}$, where $\mathcal{L}$ is the likelihood function for our model and L is an unnormalized function proportional to the likelihood:

$$\lambda = \sum_{j=1}^{N} \left(\frac{\left[z_j - \frac{cZ(H_0,R_j)+V_{jr}}{c}\right]^2}{\sigma_{zj}^2} + \frac{\left[\dot{\phi}_j - \frac{V_{j\phi}}{R_{jA}\sin(\theta_j)}\right]^2}{\sigma_{\dot{\phi}_j}^2} + \frac{\left[\dot{\theta}_j - \frac{V_{j\theta}}{R_{jA}}\right]^2}{\sigma_{\dot{\theta}j}^2} \right) \quad (1)$$

As usual, the likelihood is the probability density of the observed data, given a set of theoretical parameters. In the above expression, the observed data are z_j (the redshift) and $\dot{\phi}_j$ and $\dot{\theta}_j$ (which describe the proper motion). The theoretical parameters are the Hubble parameter H_0, the comoving distances $\{R_j\}$, and the peculiar velocities $\{\vec{v}_j\}$. (The angular diameter distances $\{R_{jA}\}$ are determined by $\{R_j\}$ and H_0 so are not independent parameters.) The other quantities appearing in this expression, specifically the measurement uncertainties $\sigma_{\dot{\theta}_j}, \sigma_{\dot{\phi}_j}, \sigma_{z_j}$, are assumed to be known. Recall that θ_j and ϕ_j, measurements of the angular position, are assumed to be known perfectly. We therefore treat all of these values as constants. This leaves H_0, $\{R_j\}$, and $\{\vec{v}_j\}$ as the parameters in our model.

Our model considers all of the galaxies to be independent of each other, so the likelihood function for a given galaxy and set of parameters depends only on the measurements for that galaxy. Thus,

$$L(H_0, \{R_j\}, \{\vec{v}_j\}) = \prod_{j=1}^{N} L_j(H_0, R_j, \vec{v}_j), \quad (2)$$

where $L_j = e^{-\frac{1}{2}\lambda_j}$ and λ_j is the j^{th} term in the sum λ.

To determine our prior, we assume that the proper volume density of galaxies is uniform and that peculiar velocities have independent components drawn from a normal distribution with mean zero and standard deviation σ_v.

Since we assume that galaxies are drawn at random within our survey volume, the prior $P_j(H_0, R_j)$ on H_0 and R_j satisfies $dP_j \propto nR_j^2 dR_j$, where n is the number density of galaxies in redshift space. This density is proportional to H_0^3 in real space, so $dP \propto H_0^3 R_j^2 dR_j$. Our model assumes that all of the galaxies are independent of each other, so the prior on H_0 and $\{R_j\}$ is the product of the individual

[4] The angular diameter distance is the distance to an object such that the usual geometric relation $s = d\theta$ is obeyed, where d is the angular diameter distance, θ is the angular size, and s is the physical size. The comoving distance is a distance in coordinates that are chosen to compensate for the expansion of the Universe - i.e., a galaxy's comoving distance is unchanged if and only if the relative velocity between the galaxy and the observer is solely due to the expansion of the Universe. For cosmological distances, these two values may not be the same.

priors:

$$dP(H_0,\{R_j\}) = \prod_{j=1}^{N} dP_j(H_0,R_j) \propto \prod_{j=1}^{N} H_0^3 R_j^2 dR_j. \quad (3)$$

Furthermore, our assumptions about the distribution of peculiar velocity components lead to a peculiar velocity prior

$$P(\{\vec{v}_k\}) = \prod_{j=1}^{N} P_j(\vec{v}_j) = \prod_{j=1}^{N} e^{\frac{-||\vec{v}_j||^2}{2\sigma_v^2}}. \quad (4)$$

(See Section 4.5 for further discussion of galaxy peculiar velocities.) Therefore the unnormalized posterior probability distribution for the survey becomes

$$A(H_0,\{R_j\},\{\vec{v}_j\}) \propto \prod_{j=1}^{N} H_0^3 R_j^2 e^{\frac{-||\vec{v}_j||^2}{2\sigma_v^2}} L_j(H_0,R_j,\vec{v_j}). \quad (5)$$

The peculiar velocities $\{\vec{v}_j\}$ are nuisance parameters, so we perform an analytic marginalization. The marginalized likelihood is $\prod_j B_j$, where

$$B_j(R_j,H_0) \propto H_0^3 R_j^2 \iiint_{-\infty}^{+\infty} e^{\frac{-||\vec{v}_j||^2}{2\sigma_v^2}} L_j \, dv_{jr}\, dv_{j\phi}\, dv_{j\theta}. \quad (6)$$

This yields

$$B_j(R_j,H_0) \propto H_0^3 R_j^2 e^{-\frac{1}{2}\beta_j}, \quad (7)$$

where

$$\begin{aligned}\beta_j(R_j,H_0) = -\ln&\left(\frac{R_{jA}^4}{(\sigma_v^2+R_{jA}^2\sigma_{\dot{\theta}j}^2)(\sigma_v^2\csc^2(\theta_j)+R_{jA}^2\sigma_{\dot{\phi}j}^2)}\right)\\ &+\frac{(-cZ(H_0,R_j)+v_{0r}+cz_j)^2}{\sigma_v^2+c^2\sigma_{zj}^2}+\frac{(\dot{\theta}_j R_{jA}+v_{0\theta})^2}{\sigma_v^2+R_{jA}^2\sigma_{\dot{\theta}j}^2}\\ &+\frac{(\dot{\phi}_j R_{jA}+\csc(\theta_j)v_{0\theta})^2}{\csc^2(\theta_j)\sigma_v^2+R_{jA}^2\sigma_{\dot{\phi}_j}^2}. \end{aligned} \quad (8)$$

The distances $\{R_j\}$ are also nuisance parameters, so we marginalize over them as well. This integral cannot be done analytically, so we resort to numerical methods. Fortunately, the independence of the galaxies means that we can write the N-dimensional integral as a product of N one-dimensional integrals. Thus, our final expressions for the posterior probabilities $\{\mathcal{L}_j\}$ have only H_0 as a parameter:

$$\mathcal{L}_j(H_0) \propto \int_0^{\infty} B_j(R_j,H_0)dR_j \quad (9)$$

Therefore

$$\mathcal{L}(H_0) \propto \prod_{j=1}^{N} \mathcal{L}_j(H_0), \quad (10)$$

so we now have an expression for our posterior probability distribution $\mathcal{L}$ marginalized over all nuisance parameters.

3.3 Fisher Information

The Fisher information of a set of random variables is a measure of how much information these variables contain about an unknown parameter. It therefore provides a useful way to quantify the uncertainty of a method of parameter estimation. Indeed, for unbiased estimators, the Cramér-Rao inequality (discussed below) uses the Fisher information to set a strict lower bound on the variance of the estimator.

For a single parameter H_0 and posterior probability distribution $\mathcal{L}(H_0)$, the Fisher information $F(H_0)$ is given by

$$F(H_0) = \left\langle -\frac{d^2\ln(\mathcal{L}(H_0))}{dH_0^2}\right\rangle. \quad (11)$$

Since the measurements for different galaxies are independent, we know that the Fisher information for a sample of N galaxies is $F_N(H_0) = NF_j(H_0)$, where $F_j(H_0)$ is the Fisher information for a single galaxy. Thus, we may concern ourselves with calculating only $F_j(H_0)$, which is

$$F_j(H_0) = \left\langle -\frac{d^2\ln(\mathcal{L}_j(H_0))}{dH_0^2}\right\rangle. \quad (12)$$

We therefore wish to compute

$$\left\langle -\frac{d^2\ln(\mathcal{L}_j(H_0))}{dH_0^2}\right\rangle = \left\langle -\frac{\mathcal{L}_j(H_0)\frac{d^2\mathcal{L}_j}{dH_0^2} - \left(\frac{d\mathcal{L}_j}{dH_0}\right)^2}{\mathcal{L}_j(H_0)^2}\right\rangle. \quad (13)$$

We compute this value via Monte-Carlo integration: for a fixed set of experimental parameters, we randomly generate many sets of data (with a uniform proper volume density) and find $-\frac{d^2\ln(\mathcal{L}_j(H_0))}{dH_0^2}$ for each, taking the mean as the expected value. This yields the Fisher information for a single galaxy, which we then multiply by N to find the Fisher information for a survey of N galaxies. To simplify this calculation, we use the low-redshift approximation $cZ(H_0,R_j) = H_0 R_j$.

Given the expected value of the Fisher information, we then compute a lower bound on σ_{H_0}, the standard deviation of the maximum-likelihood estimator of H_0, via the Cramér-Rao Inequality:

$$\sigma_{H_0} \geq \frac{1}{\sqrt{F_N(H_0)}}. \quad (14)$$

This inequality applies to any unbiased estimator of H_0. In Section 4.3, we will compare it to the maximum-likelihood estimator.

While the maximum-likelihood estimator is biased (as we will see in Section 4.3), the bias is typically small. Furthermore, the correct expression for the Cramér-Rao inequality for a biased estimator $\hat{\theta}$ of a parameter θ is

$$\mathrm{var}(\hat{\theta}) \geq \frac{(1+b'(\theta))^2}{F(\theta)}, \quad (15)$$

where $b(\theta)$ is the bias and $F(\theta)$ is the Fisher information (Jaynes 2003). In the case where $b'(\theta)$ is small, this lower bound is well-approximated by $1/F(\theta)$. We will show in Section 4.3 that the maximum-likelihood estimator of H_0 is in such a regime, and therefore equation (14) is approximately true.

3.4 Simulation

We also compute the uncertainty in H_0 via simulation. The simulation has the advantage of allowing all redshifts and angular diameter distances to be calculated from a numerical solution of the Friedmann equation, so the low-redshift approximation does not enter into the simulation.

Given the maximum redshift of the survey, we use an interpolation of our numerical solution of the Friedmann equation to find the comoving distance that corresponds to a cosmological redshift equal to the maximum survey redshift. We then randomly generate galaxies with a uniform proper volume density throughout a sphere whose radius is twice that of the calculated comoving distance. Each galaxy is then given a random peculiar velocity, with each component drawn from a normal distribution with mean zero and standard deviation σ_v. Galaxies whose resulting redshifts exceed the redshift limit of the survey are then discarded. This process is iterated until the desired number of galaxy observations have been generated. We then assume that the two components of each galaxy's proper motion have been measured with some uncertainty σ_p. We generate the observed data by adding noise with this standard deviation to the "true" proper motion components corresponding to the given distance and peculiar velocity.

Then, given a set of data, we numerically optimize $\mathcal{L}$ to find the maximum-likelihood estimate of H_0. We repeat this for many randomly generated surveys in order to compute the expected value and standard deviation of the maximum-likelihood estimator of H_0. We take the standard deviation of the estimator to be the uncertainty in the measurement of H_0.

3.5 Velocity Field Reconstruction

The procedure described above assumes that galaxy peculiar velocities are *uncorrelated* and *unknown*. As we will describe below, we consider hypothetical surveys in which galaxies are spaced farther apart than the velocity correlation length, to reduce the effect of correlated peculiar velocities. In order to further assess the effect of these assumptions, we perform simulations in a subset of our parameter space for models in which galaxy peculiar velocities are correlated but reconstructed with some uncertainty.

The likelihood function and structure of the simulation remains essentially the same. However, in our *primary tests*, when we generate the peculiar velocities of the galaxies, we consider two parts: a correlated component due to a velocity field that is a realization of a Gaussian random process with a given coherence length, and an uncorrelated component where each component is drawn independently from a normal distribution. We further imagine that the correlated component is known and the uncorrelated component is unknown. These assumptions are meant to approximate the idea that reconstructions of peculiar velocities will do much better at determining the large-scale coherent component of the velocity field, so the unknown residual will be much less correlated.

Given the importance of velocity correlations in the actual Universe, we conducted secondary tests to verify that our treatment of velocity correlations is reasonable. The worst-case scenario for our analysis is an experiment in which the actual peculiar velocities are correlated but the analysis in the future experiment treats them as uncorrelated. We analyze this case by generating a peculiar velocity field that is a realization of a Gaussian random process with a coherence length of 50 Mpc and using this field to generate data as described in Section 3.4. We then fit H_0 to this data exactly as described in Section 3.4, as if the simulated peculiar velocities had no correlations.

3.6 Extragalactic Statistical Parallax

In most cases of interest, the most useful proper motion signal comes from the motion of the Earth with respect to the CMB, since we consider this to be perfectly known. However, there is in principle another effect in the signal, which we will describe as extragalactic statistical parallax. This effect is due to the peculiar velocities of the observed galaxies; while each peculiar velocity is unknown, we have assumed that we know the distribution they are drawn from. This knowledge of a typical peculiar velocity lets us estimate a typical distance for a galaxy (given its proper motion). With this distance and the redshift, we can then estimate H_0.

This effect necessarily has a large uncertainty (due to the fact that peculiar velocities are unknown). As a result, the effect is often small compared to the signal provided by the known motion of the Earth.

However, in some cases, this statistical effect is as important as (or even more important than) the proper motion due to actual parallax. For example, in cases where the proper motion due to the Earth's motion is small compared to the uncertainty in proper motion measurements (either because of high uncertainty or large distances), the signal due to Earth's motion is weak. As a result, the signal is dominated by this extragalactic statistical parallax effect, and an increase in the peculiar velocity dispersion actually leads to a decrease in the uncertainty on the measurement of H_0. This is discussed further in Section 4.6.

4 RESULTS

4.1 Cosmological Parameters

We used the following cosmological parameters in the Fisher information analysis and in the simulation.

The current radiation energy density parameter was set to $\Omega_R = 9 \times 10^{-5}$. The current matter energy density parameter was set to $\Omega_M = 0.31$. The current dark energy density parameter Ω_Λ was set to $1 - \Omega_R - \Omega_M$, rendering the Universe flat (Ryden 2016; Planck Collaboration et al. 2020).

In this section, we analyze a survey of a universe with Hubble parameter equal to $H_0 = 70$ km s^{-1} Mpc^{-1}, galaxy peculiar velocity dispersion equal to $\sigma_v = \frac{660}{\sqrt{3}}$ km/s (Padilla & Lambas 1999), and speed of the solar system relative to the CMB equal to $\langle 25.8$ km/s, 246 km/s, 271 km/s$\rangle$ in standard Galactic coordinates (Gordon et al. 2008).

Throughout this analysis, we hold the fractional uncertainty in measured redshift fixed at 0.001. Each galaxy is assumed to have the same uncertainty σ_p in both components of its proper motion.

4.2 Trials

To relate comoving distances to cosmological redshifts, we numerically solved the Friedmann equation at fifty evenly spaced redshift values between 0 and 1 and then used these points to interpolate the relationship throughout the simulation.

The Monte Carlo integration in the Fisher analysis was performed with 1 00000 points.

The simulation generated between 1000 and 10000 surveys for a given set of experimental parameters (depending on the point in parameter space). From these surveys, the standard deviation of the maximum-likelihood estimates of H_0 was taken as the uncertainty in H_0 and the mean value of the maximum-likelihood estimates was taken as the expected value of H_0.

All numerical optimizations were performed with SciPy's Powell optimization method, and all numerical integrations were performed with SciPy's quadrature integration method.

To ensure that each simulation generated enough surveys for reliable results, we ran the simulation twice for each point in parameter space and compared the percent error in the uncertainty estimates of the two runs. The maximum percent error was 4.92%. The minimum percent error was 2.05×10^{-6}%. The mean percent error was 1.30%, and the standard deviation of the percent errors was 1.14%.

4.3 Fisher Analysis Results

As mentioned in Section 3.3, the Cramér-Rao Inequality requires an unbiased estimator to be guaranteed. Figure 1 shows that the maximum-likelihood estimator has a slight negative bias, which is always small compared to the uncertainty. The ratio of the bias in estimated H_0 to the error in H_0 ranges from -0.03 to -0.2, with a median of -0.08. However, this ratio is smaller for low ΔH_0 values than for higher ones, typically by a factor of roughly 2. The bias is therefore relatively small for the results of interest.

A possible explanation for this bias is the volume element in our prior and our assumption about uniform volume density of galaxies. All else being equal, our model prefers larger distances for galaxies. This is simply because there is more volume at larger distances - if we know nothing else about a galaxy, it is more likely to be found at larger distances because of the higher volume and uniform density. The estimator therefore tends to select the largest distance compatible with the redshift observation. For a fixed redshift, increasing the distance corresponds to a reduced H_0, producing the effect we observe. While this is a reasonable explanation for the effect, one should also bear in mind that an estimator has no guarantee of being unbiased. An exact explanation of the source of the bias does not necessarily exist.

As discussed in Section 3.3, the Cramér-Rao lower bound for a biased estimator is well approximated by the reciprocal of the Fisher information when the derivative of the bias with respect to the estimator is low. This is typically the case for our estimator; for example, we numerically estimated the derivative of the bias at $H_0 = 70$ km s^{-1} Mpc^{-1} with $\sigma_p = 0.211$ μas yr^{-1}, $N = 216$, and a maximum survey redshift of 0.070, finding it to be approximately $b'(H_0) = 0.0088$. Since $b'(H_0) \ll 1$, the correct value for the Cramér-Rao lower bound is very close to the reciprocal of the Fisher information. We therefore use the unbiased version of the Cramér-Rao inequality to quantify the standard deviation of our estimator, taking the reciprocal of the square root of the Fisher information to be the estimate of the uncertainty in H_0.

For each point that we simulated in parameter space, we estimated the uncertainty in H_0 using the Fisher information. The set of ratios of simulation uncertainty estimation to Fisher uncertainty estimation (as given by equation (14)) had a minimum of 0.926, a maximum of 1.151, a mean of 1.042, and a standard deviation of 0.029. In summary, the uncertainty in the maximum-likelihood estimator is always extremely close to the Cramér-Rao bound.

4.4 Simulation Results

We imagine a survey with a fixed number of galaxies, a maximum survey redshift, and desired error tolerance in the determination of H_0. We then use the results of the simulation to interpolate the necessary precision of proper motion measurement (σ_p) required to meet this error tolerance.

For each redshift limit, we limit the number of galaxies such that the average distance between galaxies in the simulation is greater than or equal to the velocity coherence length, which we take to be 50 Mpc.

We chose this value based on data from the Galacticus simulation from the CosmoSim suite of simulations (Knebe et al. 2017; Benson 2012). Peculiar-velocity correlations in these simulations appear to be broadly consistent with observational data (Wang et al. 2018).

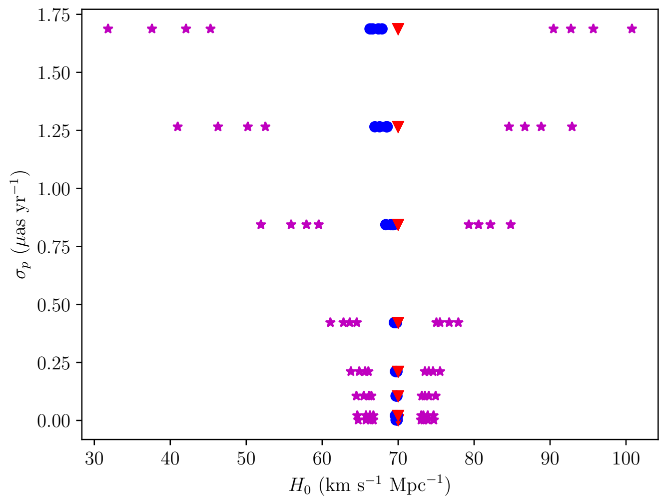

Figure 1. This plot displays the bias for a set of survey parameters with the maximum survey redshift held fixed at 0.058, where σ_p is the proper motion uncertainty. The red triangles mark the true value of H_0 in the simulation, 70 km s^{-1} Mpc^{-1}. The blue points mark the expected value of the maximum-likelihood estimator of H_0 for the simulation of a given parameter set. The magenta stars mark the mean value minus the standard deviation and the mean value plus the standard deviation. The different points for the same proper motion uncertainty correspond to surveys with different numbers of galaxies ranging from 50 to 125.

For our purposes, a simulation-based estimate is cleaner than an observational result, as we are interested in knowing the correlation function of arbitrary components of the 3D peculiar velocity field. Due to both cosmic variance and the fact that only radial components can typically be measured, the relationship between this quantity and observational data is complicated. In any case, for present purposes a reasonable estimate of the coherence length is all that is required.

To be specific, we computed the two-point velocity correlation function for each component of galaxy velocities for a cubic neighborhood of CosmoSim data and found the distance by which the two-point correlation function had dropped by approximately one e-fold. This cubic neighborhood had a proper side length of 150 Mpc and roughly 35000 galaxies of mass at least $10^{12} M_\odot$ within it.

Figure 2 displays the required sensitivity in term of a figure of merit,

$$\mathrm{FOM} = \frac{\sigma_p}{N^{1/2}}, \tag{16}$$

where σ_p is the proper motion uncertainty and N is the number of galaxies surveyed. Under the assumption that the precision of a proper motion measurement improves in proportion to the square root of the observing time, this FOM is proportional to $T^{-1/2}$, where T is the total observing time devoted to the survey.[5] Larger FOMs therefore correspond to “easier" surveys.

4.5 Velocity Field Reconstruction Results

As described in Section 3.5, we compared the results of the uncorrelated survey to the results of the survey with velocity field recon-

[5] Note that T is the telescope time, not the total elapsed time, for the survey. Proper motion measurements will improve in direct proportion to the total elapsed time. Our figure of merit assumes that the latter is fixed.

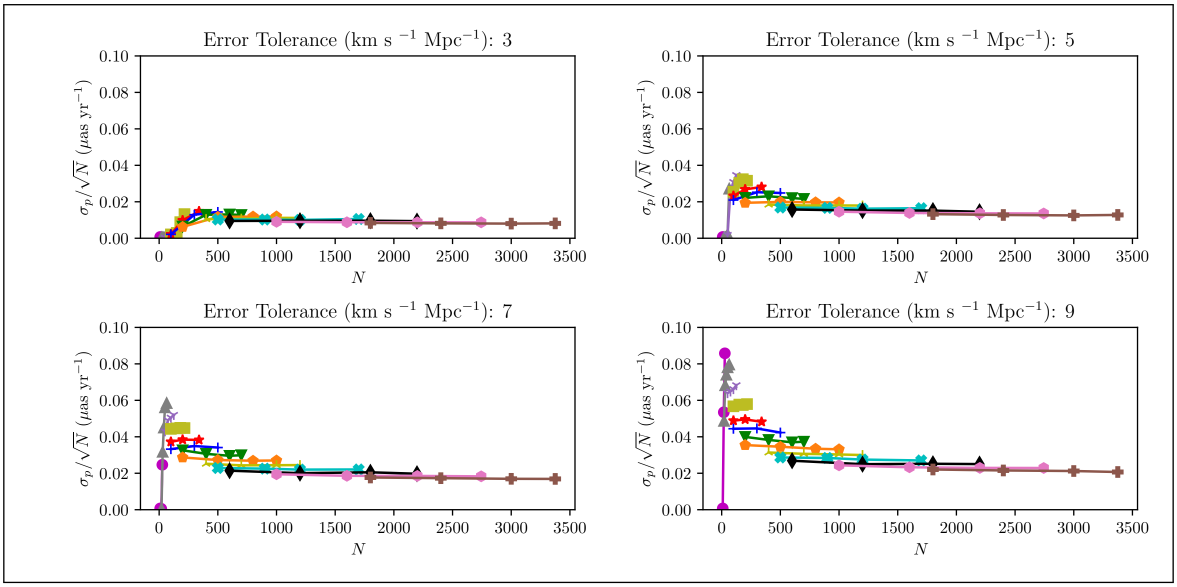

Figure 2. The figure of merit is graphed versus number of galaxies for a specified error tolerance in H_0, where σ_p is the proper motion uncertainty and N is the number of galaxies surveyed. The different colors of lines correspond to different maximum survey redshifts as follows: 0.035 (magenta), 0.046 (gray), 0.058 (purple), 0.070 (olive), 0.081 (red), 0.093 (blue), 0.104 (green), 0.116 (orange), 0.128 (yellow), 0.139 (cyan), 0.151 (black), 0.162 (pink), 0.174 (brown). For each maximum redshift, the maximum value of N is determined by the requirement that galaxy separations exceed the velocity correlation length.

Table 1. Ratios of error estimates based on the assumption of uncorrelated errors to those based on the assumption that 75% of the peculiar velocity variance is correlated and has been reconstructed, as described in Section 3.5.

Max Redshift Redshift	Min Ratio	Max Ratio	Mean Ratio	Standard Deviation
0.035	1.15	1.59	1.38	0.16
0.046	1.17	1.60	1.39	0.14
0.058	1.17	1.62	1.40	0.14

structions. For the subset of parameter space with redshift limits of 0.058 and below, we compute the uncertainty in H_0 via simulations in which 0.25, 0.5, and 0.75 of the variance of peculiar velocity components is due to this known and correlated velocity field. The σ_v^2 used in the likelihood function is therefore the fraction of the variance attributable to the random component of the velocity.

We found the ratio of the error estimate of the uncorrelated simulation to the error estimate of the simulation with 0.75 of the velocity having been reconstructed. We then computed the maximum, minimum, mean, and standard deviation of these ratios. The results are found in Table 1.

Figure 3 shows FOM plots under the assumptions that the fraction of peculiar velocities that are correlated and reconstructed is 0.25, 0.50, and 0.75.

The differences resulting from peculiar velocity reconstruction are small, providing evidence that peculiar velocity correlations do not dramatically affect our results.

In addition to the primary tests described above, we performed additional tests as described in Section 3.5. We now detail the results of these additional tests.

Given the peak in Figure 2, we are primarily interested in the lower redshift surveys. We therefore analyzed the worst-case scenario (of correlated velocities with correlation completely ignored in the fitting of H_0) for the same survey sizes and proper motion uncertainties as the original data set for the lower redshift surveys. For the subset of the parameter space which we analyzed in this worst case scenario, the ratio of ΔH_0 in the worst case scenario to ΔH_0 in the original analysis had a mean of 1.85, a minimum of 1.04, a maximum of 3.41, and a standard deviation of 0.60.

Figures 4 and 5 display H_0 error estimates as a function of parameter space for both our original and worst case analysis. Figure 4 shows these estimates for a slice of parameter space, while 5 shows these estimates for all points in parameter space which were analyzed using both methods. The comparison of these results shows that while our approximation of uncorrelated velocities is not a negligible error, it still gives us both the correct shape of the parameter space and estimates of the H_0 uncertainty that are typically within a factor of two. These similarities support our claim that our approximation is good enough to draw useful conclusions about the order of magnitude of errors involved in a future parallax survey and about the optimal design of such a survey.

4.6 Extragalactic Statistical Parallax Results

To illustrate the information obtainable from "statistical parallax," we performed simulations in which the Earth's peculiar velocity was set to zero, so that there is no overall secular parallax. The results are shown in Figure 6.

Comparison of Figure 6 to Figure 2 shows that in the simulation with uncorrelated velocities, a significant fraction of the signal is due to statistical parallax. However, this comparison presumably overestimates the effect of statistical parallax in relation to actual secular parallax. First, the assumption that peculiar velocities are completely unknown causes an underestimation of the signal due to well-known motions. See Figure 3 and note that as the fraction of reconstructed peculiar velocity increases, the uncertainty in H_0 decreases. Second, the assumption that peculiar velocities are uncorrelated most likely causes an overestimation of the signal due to statistical parallax. Since all of the information in statistical parallax is due to knowl-

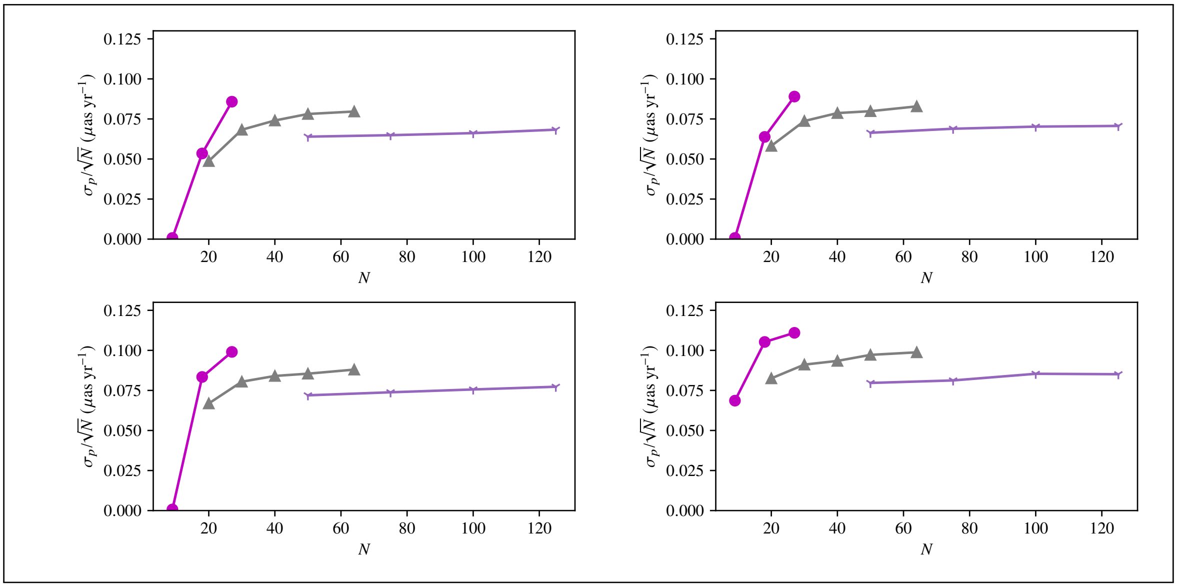

Figure 3. The figure of merit is graphed versus number of galaxies for an error tolerance in H_0 of 9 km s^{-1} Mpc^{-1}, where σ_p is the proper motion uncertainty and N is the number of galaxies surveyed. The upper left panel has 0 of the peculiar velocity reconstructed, the upper right panel has 0.25 of the peculiar velocity reconstructed, the lower left panel has 0.5 of the peculiar velocity reconstructed, and the lower right panel has 0.75 of the peculiar velocity reconstructed. The colors are as in Figure 2.

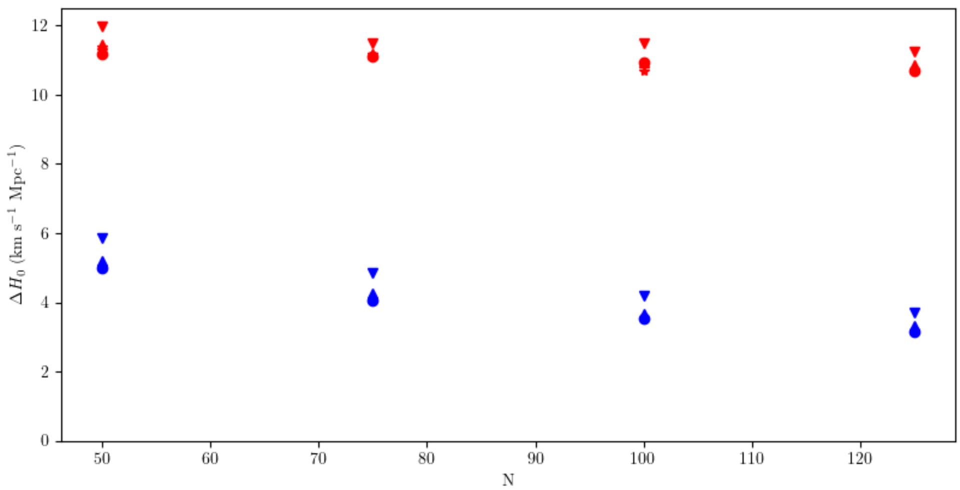

Figure 4. The uncertainty in H_0 is graphed versus number of galaxies for various values of σ_p (corresponding to the different curves). The blue curves correspond to the original analysis; the red curves correspond to the worst case scenario analysis. Each σ_p value is associated with a specific indicator, so the red and blue curves with the same indicators are for the same σ_p values.

edge of the statistical distribution of peculiar velocities, correlating the velocities presumably results in less information from the same number of galaxies.

Unfortunately, statistical parallax in the actual Universe would be significant in the case where velocity correlations are important but unknown. This scenario is not well approximated by either of the simulations: the first simulation has uncorrelated peculiar velocities, while the second simulation has known correlations. We therefore cannot test a more realistic case of statistical parallax using this model, so we cannot test the hypothesis that uncorrelated peculiar velocities leads to an overestimate of the usefulness of statistical parallax.

5 DISCUSSION

The plots in Figure 2 have the same general features, several of which are to be expected. For each error tolerance, the FOM has a clear peak at a maximum redshift between 0.045 and 0.058, caused by competing effects. If the redshift limit is small, there is not enough volume to survey a large number of galaxies while maintaining the constraint that galaxy separation exceed the correlation length. (This

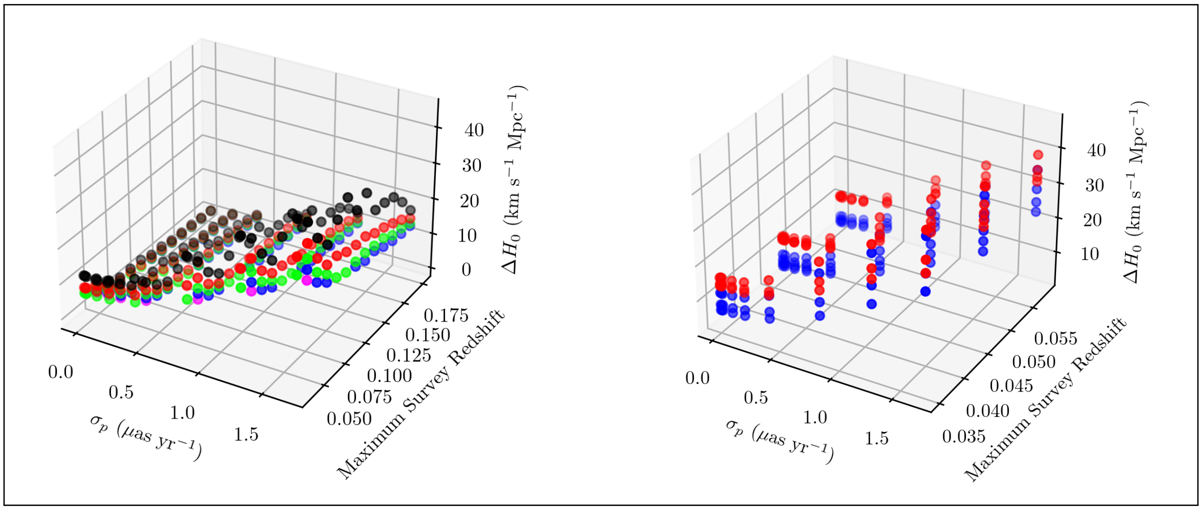

Figure 5. The uncertainty ΔH_0 in the measurement of the Hubble constant is plotted as a function of the survey parameters. The proper motion uncertainty σ_p and the maximum survey redshift are displayed on the axes. In the left plot, different survey sizes for these parameters are indicated by different colored dots. These results are for the entirety of parameter space in the original analysis. In the right plot, the blue points correspond to the original analysis while the red points correspond to the worst case analysis. These results are for the subset of parameter space analyzed via both methods. The multiple points occurring at any given σ_p and maximum redshift correspond to different survey sizes.

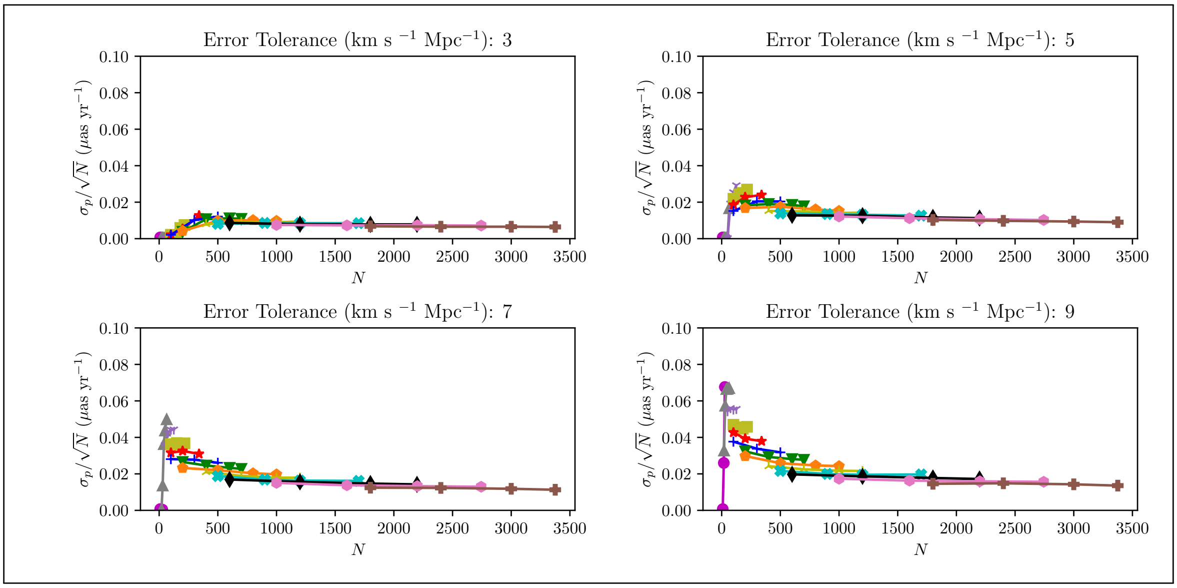

Figure 6. The figure of merit is graphed versus number of galaxies for a specified error tolerance in H_0, where σ_p is the proper motion uncertainty and N is the number of galaxies surveyed. In contrast to Figure 2, our Galaxy's peculiar velocity is set to zero, so that only the effects of extragalactic statistical parallax are included. The colors are as in Figure 2.

is the reason that the low-redshift curves stop at small values of N.) At high redshift, on the other hand, the parallax signal becomes small and hard to measure.

A useful observation for experimental design is the relative scale of the curve and the steepness of the two sides. While there is a clear peak in the figure of merit, it is within a factor of roughly four of the figure of merit for the higher redshift limits that we tested – that is, the peak FOM is of the same order of magnitude as those with greater redshift limits. Furthermore, the curve is much steeper to the left of the peak than to the right. This indicates that if a survey design is to deviate from the ideal redshift limit, it is better for the redshift limit to be higher than the ideal redshift limit than for it to be lower.

Although our formalism does not allow us to forecast errors for surveys in which galaxies are closer together than the velocity correlation length, there is reason to believe that the error forecasts for surveys with larger numbers of more closely-spaced galaxies would have similar FOMs – that is, that the curves in Figure 2 and the following figures would roughly plateau rather than decline dramatically if extended to higher N at a fixed redshift cutoff. In particular, in the limit where the separation between a set of galaxies is much less than the velocity correlation length, we could treat the peculiar velocities as identical and treat the entire collection as a single object with a correspondingly larger observing time. In this limit, the FOM is independent of the number of galaxies in that collection. To forecast errors for a survey with mean galaxy separation less than the correlation length, we could imagine dividing the survey volume into voxels whose size is of order the correlation length and treating all galaxies in each voxel as a single data point in this manner. (Of course, one would not analyze the real data in this way, but it is plausible that such an approach would give decent enough error forecasts for present purposes.) This approximation would lead to plateaus in the various curves – that is, one would achieve results similar to the optimum FOM even if one shifted to larger values of N at a given redshift limit.

Finally, we wish to compare the precision of measurement required for a useful constraint of H_0 with the capabilities of present and near-future experiments. For example, with an error tolerance of 7 $\mathrm{km\,s^{-1}\,Mpc^{-1}}$, the optimum FOM is $\sim 0.06\,\mu\mathrm{as\,yr^{-1}}$, obtained by surveying ~ 64 galaxies with redshift limit ~ 0.046. This corresponds to a precision for each measurement of $\sigma_p \sim 0.5\,\mu\mathrm{as\,yr^{-1}}$. While this is certainly a greater degree of precision than is currently available, it is not vastly beyond the capabilities of current astrometric surveys. For example, Paine et al. (2020) forecast a Gaia end-of-mission catalog with 10^4 nearby galaxies with mean proper motion uncertainties of about 70 $\mu\mathrm{as\,yr^{-1}}$, leading to an FOM of about $0.7\,\mu\mathrm{as\,yr^{-1}}$, about a factor of ten greater than our optimal forecast. However, it should be noted that Gaia's primary mission is to catalogue Milky Way objects and their proper motions; measurement of H_0 is not a primary science goal (de Bruijne 2012). In this sense, then, the measurements needed to constrain H_0 via extragalactic parallax are not too far beyond current capabilities. In the future, instruments such as the Nancy Grace Roman Space Telescope (Mutchler et al. 2021), the Vera C. Rubin Observatory (Ivezić et al. 2019), or the next-generation VLA (McKinnon et al. 2019) may provide the capability to perform even better surveys.

As we noted in the introduction, the calculations presented in this paper are meant as preliminary estimates. Although they are based on approximations that limit the precision of the error forecasts, we have presented tests that show that the resulting errors are not so large as to prevent our results from providing a useful guide at this early stage of consideration of this method. Naturally, as details of a survey design come into focus, more precise error forecasts will be required.

The methods we have presented here can be extended in various ways to assist in designing the optimum design for a future proper motion survey. For example, we have assumed an all-sky redshift-limited survey, but our simulations can easily be generalized to accommodate partial sky coverage or more complicated redshift and/or brightness selection functions. In future work, we plan to consider whether including the strongly lensed galaxies that are expected to be found in future surveys (Oguri & Marshall 2010) can enhance the precision of the measurement, by increasing the size of the proper motion of some images and/or by using multiple images to reduce the uncertainty.

ACKNOWLEDGEMENTS

I would like to thank Dr. Ted Bunn for his excellent mentorship throughout this project and, more generally, my time at the University of Richmond. I would also like to thank Dr. Christine Helms and Dr. Matt Trawick for their helpful comments.

This work was supported by an Undergraduate Science Research Fellowship grant from the Virginia Foundation of Independent Colleges as well as by the University of Richmond. The CosmoSim database used in this paper is a service by the Leibniz-Institute for Astrophysics Potsdam (AIP).

DATA AVAILABILITY

No new observational data were obtained as part of this work. Code used in the computations is available upon request to the authors.

REFERENCES

Adler R. J., Casey B., Jacob O. C., 1995, American Journal of Physics, 63, 620
Bachchan R. K., Hobbs D., Lindegren L., 2016, A&A, 589, A71
Benson A. J., 2012, New Astronomy, 17, 175
Croft R. A. C., 2021, MNRAS, 501, 2688
DES Collaboration et al., 2022, Dark Energy Survey Year 3 Results: Constraints on extensions to ΛCDM with weak lensing and galaxy clustering (arXiv:2207.05766)
Darling J., Truebenbach A. E., 2018, ApJ, 864, 37
Darling J., Truebenbach A., Paine J., 2018, in Murphy E., ed., Astronomical Society of the Pacific Conference Series Vol. 517, Science with a Next Generation Very Large Array. p. 813 (arXiv:1807.06670)
Ding F., Croft R. A. C., 2009, MNRAS, 397, 1739
Freedman W. L., et al., 2019, The Astrophysical Journal, 882, 34
Gordon C., Land K., Slosar A., 2008, MNRAS, 387, 371
Hall A., 2019, MNRAS, 486, 145
Hinshaw G., et al., 2009, ApJS, 180, 225
Hogg D. W., 1999, arXiv e-prints, pp astro–ph/9905116
Ivezić Ž., et al., 2019, ApJ, 873, 111
Jaynes E. T., 2003, Probability theory: The logic of science. Cambridge University Press, Cambridge
Kamionkowski M., Riess A. G., 2022, The Hubble Tension and Early Dark Energy (arXiv:2211.04492)
Kardashev N. S., 1986, Soviet Ast., 30, 501
Knebe A., et al., 2017, Monthly Notices of the Royal Astronomical Society, 474, 5206
Lazovik Y. A., Rastorguev A. S., Zabolotskikh M. V., Gorynya N. A., 2019, The period-luminosity relation for Cepheids derived from multiphase temperature measurements and Cepheids kinematics based on GAIA DR2 data (arXiv:1911.13102)
Luri X., et al., 2018, A&A, 616, A9
McKinnon M., Beasley A., Murphy E., Selina R., Farnsworth R., Walter A., 2019, in Bulletin of the American Astronomical Society. p. 81
McQuinn K. B. W., Boyer M., Skillman E. D., Dolphin A. E., 2019, The Astrophysical Journal, 880, 63
Mutchler M., et al., 2021, in American Astronomical Society Meeting Abstracts. p. 216.01
Oguri M., Marshall P. J., 2010, MNRAS, 405, 2579
Padilla N., Lambas D. G., 1999, Monthly Notices of the Royal Astronomical Society, 310, 21
Paine J., Darling J., Graziani R., Courtois H. M., 2020, ApJ, 890, 146
Planck Collaboration et al., 2020, A&A, 641, A6
Riess A. G., Casertano S., Yuan W., Macri L. M., Scolnic D., 2019, ApJ, 876, 85
Riess A. G., et al., 2022, The Astrophysical Journal Letters, 934, L7
Ryden B., 2016, Introduction to Cosmology, 2 edn. Cambridge University Press
Truebenbach A. E., Darling J., 2017, ApJS, 233, 3
Wang Y., Rooney C., Feldman H. A., Watkins R., 2018, Monthly Notices of the Royal Astronomical Society, 480, 5332
Wright B. S., Li B., 2018, Physical Review D, 97
Yuan W., et al., 2022, The Astrophysical Journal, 940, 64
de Bruijne J. H. J., 2012, Astrophysics and Space Science, 341, 31

This paper has been typeset from a TEX/LATEX file prepared by the author.